Number 3 Volume 16 September 2010 Journal of Engineering

DEVELOPING LAMINAR MIXED CONVECTION HEAT TRANSFER THROUGH CONCENTRIC ANNULI

Asst. Prof. Dr. Ihsan Y. Hussain
Mechanical Engineering Department
University of Baghdad

Mohammed Abdul Raouf Nima Al-Safi
Mechanical Engineering Department
University of Baghdad

ABSTRACT

Theoretical and experimental study has been conducted on developing laminar mixed convection heat transfer air flow through an annulus for both aiding and opposing flow with uniformly heated inner cylinder and adiabatic outer cylinder for the theoretical part and with uniformly heated inner cylinder while the outer cylinder is subjected to the ambient for the experimental part. In the theoretical investigation the energy equation was first solved using (ADI) method, and then the momentum equations and continuity equation were combined as the pressure correction formula and solved by the SIMPLE algorithm. The present theoretical work covers Ra range from $4.55*10^5$ to $5.649*10^6$ and Re range from 300 to 1000 with radius ratio of 0.555 and Pr=0.72. The velocity and temperature profile results have revealed that the secondary flow created by natural convection have significant effects on the heat transfer process and the results reveal an increase in the Nusselt number values as Ra increases. The experimental setup consists of an annulus which has a radius ratio of 0.555 and inner cylinder with a heated length 1.2m subjected to a constant heat flux while the outer cylinder is subjected to the ambient temperature. The investigation covers Reynolds number range from 154 to 724, heat flux varied from 93 W/m^2 to 857 W/m^2, and annulus angles of inclinations $\alpha=0°$ (horizontal), $\alpha=20°$, 60° (inclined aiding flow), $\alpha=-20,-60$ (inclined opposing flow) and $\alpha=90°$ (vertical). The experimental results show an increase in the local Nusselt number values as the heat flux increases and as the angle of the inclination moves from the positive angles (inclined aiding flow) to the horizontal position and from the negative angles (inclined opposing flow) to the horizontal position. The experimental results show that the local Nusselt number values of the aiding flow are higher than that of the opposing flow at the same Reynolds number and heat flux.

الخلاصة

أُجريتْ دراسة نظرية و عملية لانتقال الحرارة بالحمل المختلط لجريان الهواء خلال تجويف حلقي ذو أسطوانتين متمركزتين (في حالة الجريان الثانوي باتجاه الجريان الرئيسي وفي حالة الجريان الثانوي عكس اتجاه الجريان الرئيسي)؛ الداخلية مسخنة تسخين منتظم و الخارجية معزولة في حالة الدراسة النظرية اما في حالة الدراسة العملية فان الاسطوانة الداخلية مسخنة تسخين منتظم والخارجية معرضة الى درجة حرارة الجو. في البحث النظري تم حل معادلة الطاقة اولا باستخدام طريقة (ADI) ثم تم ربط معادلات الزخم بمعادلة

الاستمرارية لانتاج معادلة تصحيح الضغط والتي تم حلها باستخدام خوارزمية (SIMPLE). رقم رينولدز Re المستخدم في هذا البحث النظري من 300 إلى 1000 أما رقم رالي Ra من $4.55*10^5$ الى $5.649*10^6$ مع نسبة نصف قطر تساوي 0.555 وهي نفسها المستخدمة في الجزء العملي من هذا البحث ورقم براندتل Pr=0.72. اظهرت نتائج توزيع السرعة و درجات الحرارة ان الجريان الثانوي الناتج من الحمل الحر(الطبيعي) له تاثير مهم على عملية انتقال الحرارة كما اظهرت النتائج زيادة في قيم رقم نسلت الموقعي عند زيادة رقم رالي Ra. البحث العملي تضمن اجراء تجارب عملية لدراسة انتقال الحرارة الموقعي و المعدّل بالحمل المختلط لجريان الهواء المشكّل تراكبياً (أي تزامن التشكيل الحراري مع التشكيل الهيدروديناميكي) بتجويف حلقي بين اسطوانتين متحدتي المركز، نسبة نصف القطر لهما تعادل 0.555 و بطول كلي 1.2 m ، بالوضع الأفقي، المائل(في حالة الجريان الثانوي باتجاه الجريان الرئيسي وفي حالة الجريان الثانوي عكس اتجاه الجريان الرئيسي)، و العمودي. سخنت الاسطوانة الداخلية تحت فيض حراري ثابت ، بينما عرّضت الاسطوانة الخارجية إلى درجة حرارة الجو. يتراوح معدّل رقم رينولدز Re في هذا البحث من 154 إلى 724 أما الفيض الحراري فيتغير من $93\ W/m^2$ إلى$857\ W/m^2$ ، و زوايا ميل التجويف الحلقي هي 0° (أفقي)، 20° ، 60° ،-20° ،-60° ، 90° (عمودي). بينت النتائج المستخرجة من البحث العملي لكل زوايا الميلان ان رقم نسلت الموقعي يزداد كلما ازداد الفيض الحراري وكذلك يزداد رقم نسلت الموقعي عند تغير زاوية ميل الانبوب الحلقي من الزوايا الموجبة (الجريان الثانوي باتجاه الجريان الرئيسي) الى الموقع الافقي وعند تغير زاوية ميل الانبوب الحلقي من الزوايا السالبة (الجريان الثانوي عكس اتجاه الجريان الرئيسي) الى الموقع الافقي. كما بينت النتائج العملية ان قيم رقم نسلت الموقعي في حالة (الجريان الثانوي باتجاه الجريان الرئيسي) هي اكبر منها في حالة (الجريان الثانوي عكس اتجاه الجريان الرئيسي) عند نفس رقم رينولدز والفيض الحراري المسلط.

KEYWORDS: Mixed Convection, Developing, Laminar, Concentric Annuli.

INTRODUCTION

Convection heat transfer involves the transfer of heat by the motion of a fluid. The term natural convection is used if this motion is caused by density variations resulting from temperature differences within the fluid. The term forced convection is used if this motion is caused by an outside force, such as a pump, blower fan and compressor. Mixed convection flow occurs when both natural and forced convection mechanisms simultaneously and significantly contribute to the heat transfer. **(Cony and El-Sharrawi 1975)**, presented the results of a finite difference analysis for incompressible laminar flow heat transfer in concentric annuli with a simultaneously developing hydrodynamic and thermal boundary layers with three radius ratios of (0.1, 0.5, and 0.9), the boundary conditions of one wall being isothermal and the outer wall adiabatic. Results show how much error can be introduced for the case of gases (Pr=0.7) if the heat transfer is calculated by assuming a fully developed profile from the entrance. This error decreases as the flow moves away from the duct entrance and approaches full development. Also results show that the local Nusselt number for the case of an isothermal inner wall and adiabatic outer wall is greater at the same dimensionless axial distance from entrance than for the case of an isothermal outer wall and adiabatic inner wall. Combined forced-free laminar convection with a flat velocity profile in the entrance region of vertical concentric annuli has been investigated by **(El-Sharrawi and Sarhan 1980)**, for three radius ratios of (0.5 , 0.8 and 0.9) and for two boundary conditions namely, the outer wall is isothermal while the inner wall is adiabatic under $-700 \leq Gr/Re \leq 1600$ and the inner wall is isothermal while the outer wall is adiabatic under $-200 \leq Gr/Re \leq 800$. The study show that when the free convection opposes the forced flow (i.e., heating with down flow or cooling with up flow) there exist a possibility of flow reversal near the heated boundary while such a flow reversal may occur near the insulated wall if the free convection is aiding the forced flow. **(Nazrul Islam , Gaitonde and Sharma 2001)**, performed a numerical as well as an experimental investigation of steady laminar mixed convection heat transfer in horizontal concentric annuli using air and water as

the working fluid. The thermal boundary condition chosen is that of uniform heat flux at the inner wall and an adiabatic outer wall. The numerical investigations were carried out with $10^4<Ra<10^8$, $1.5 \le r_o/r_i \le 10$, $0.7 \le Pr \le 5.42$ and $200 \le Re \le 1000$. It is observed that, depending on the value of Rayleigh number, the Nusselt numbers are considerably higher than the corresponding pure forced convection values over a significant portion of the annular duct.

The main aim of the present theoretical investigation is to determine the effect of Ra number, Re number and the flow direction (i.e., aiding and opposing flow) on the variation of surface temperature, Nusselt number, temperature profile and velocity profile along the annulus. The experimental study objectives are to determine the effect of the primary flow, heat flux, the effect of inclination angle and the direction of the main flow with respect to the secondary motion on the heat transfer process along the annulus for a specific range of inner cylinder heat flux and for laminar range of the air flow.

MATHEMATICAL MODELING

For an air flow in a vertical annulus, both free and forced convection effect in axial and radial directions are presented. A two-dimensional model can be used to describe the mixed convection heat transfer in a vertical annulus with inner radius r_i and outer radius r_o which has a configuration shown in **Fig.(1)**.

ASSUMPTIONS

The following assumptions are used in the modeling:

- Incompressible fluid.
- Two dimensional in (r,z) flow.
- Simultaneously developing hydrodynamic and thermal aiding flow.
- No internal heat generation and heat dissipation.
- Neglecting viscous dissipation.
- The physical properties are constant except the density in the buoyancy term of momentum equations which varies according to Boussinesq's approximation.

GOVERNING EQUATIONS

$$\frac{\partial v}{\partial r}+\frac{v}{r}+\frac{\partial u}{\partial z}=0 \tag{1}$$

$$\rho\left(\frac{\partial u}{\partial t}+v\frac{\partial u}{\partial r}+u\frac{\partial u}{\partial z}\right)=-\frac{\partial p}{\partial z}+\mu\left(\frac{\partial^2 u}{\partial r^2}+\frac{1}{r}\frac{\partial u}{\partial r}+\frac{\partial^2 u}{\partial z^2}\right)+\rho g\beta(T-T_i) \tag{2}$$

$$\rho\left(\frac{\partial v}{\partial t}+v\frac{\partial v}{\partial r}+u\frac{\partial v}{\partial z}\right)=-\frac{\partial p}{\partial r}+\mu\left(\frac{\partial^2 v}{\partial r^2}+\frac{1}{r}\frac{\partial v}{\partial r}-\frac{v}{r^2}+\frac{\partial^2 v}{\partial z^2}\right) \tag{3}$$

$$\frac{\partial T}{\partial t}+v\frac{\partial T}{\partial r}+u\frac{\partial T}{\partial z}=\hat{\alpha}(\nabla^2 T) \tag{4}$$

NONDIMENSIONALIZATION

To nondimensionalize the variables used in the governing equations, the following dimensionless variables are defined

$$R=\frac{r}{r_o},\quad Z=\frac{2z(1-N)}{r_o Re},\quad U=\frac{u}{u_i},\quad V=\frac{vr_o}{\upsilon},\quad P=\frac{p-p_i}{\rho_i u_i^{\,2}},\quad \Theta=\frac{(T-T_i)k}{q'' r_o},\quad \tau=\frac{\upsilon t}{r_o^2},$$

$$Re=\frac{u_i D_h}{\upsilon},\quad Gr=\frac{g\beta q'' r_o D_h^3}{\upsilon^2 k},\quad Pr=\frac{\mu c_p}{k}$$

DIMENSIONLESS GOVERNING EQUATIONS

$$\frac{\partial V}{\partial R}+\frac{V}{R}+\frac{\partial U}{\partial Z}=0 \tag{5}$$

$$\frac{\partial U}{\partial \tau}+V\frac{\partial U}{\partial R}+U\frac{\partial U}{\partial Z}=-\frac{\partial P}{\partial Z}+\frac{\partial^2 U}{\partial R^2}+\frac{1}{R}\frac{\partial U}{\partial R}+\frac{4(1-N)^2}{Re^2}\frac{\partial^2 U}{\partial Z^2}+\frac{Gr}{Re}\frac{\Theta}{4(1-N)^2} \tag{6}$$

$$\frac{\partial V}{\partial \tau}+V\frac{\partial V}{\partial R}+U\frac{\partial V}{\partial Z}=-\frac{Re^2}{4(1-N)^2}\frac{\partial P}{\partial R}+\frac{\partial^2 V}{\partial R^2}+\frac{1}{R}\frac{\partial V}{\partial R}-\frac{V}{R^2}+\frac{4(1-N)^2}{Re^2}\frac{\partial^2 V}{\partial Z^2} \tag{7}$$

$$\frac{\partial \Theta}{\partial \tau}+V\frac{\partial \Theta}{\partial R}+U\frac{\partial \Theta}{\partial Z}=\frac{1}{Pr}\left(\frac{\partial^2 \Theta}{\partial R^2}+\frac{1}{R}\frac{\partial \Theta}{\partial R}+\frac{4(1-N)^2}{Re^2}\frac{\partial^2 \Theta}{\partial Z^2}\right) \tag{8}$$

Entry Boundary Conditions (see **Fig.(2)**)
At Z=0 $\Theta=0$, U=1 , V=0 , P'=0 **(John D. Anderson, Jr. 1995)**

Wall Boundary Conditions (see **Fig.(2)**)
At R=N , $\partial\Theta/\partial R=-1$ (Constant heat flux). At R=1, $\partial\Theta/\partial R=0$ (Adiabatic wall)
At R=N & R=1 U=V=0 , $\partial P/\partial R=0$ **(John D. Anderson, Jr. 1995)**

Exit Boundary Conditions (John D. Anderson, Jr. 1995) (see **Fig.(2)**)
U & V (allowed to float, using zeroth-order extrapolation), P'=0

Local and Average Nusselt Number

The heat flux is computed from the following equation:

$$q_w=-k\frac{\partial T}{\partial r}\Big)_{r=ri} \tag{9}$$

The heat flux at inner wall surface equals the heat transferred by convection from this surface to the fluid that is represented by the following equation:

$$q_w=h(T_w-T_b) \tag{10}$$

By equating **eqs.(9)** and **(10)**, the heat transfer coefficient can be calculated as follows:

$$h(T_w-T_b)=-k\frac{\partial T}{\partial r}\Big)_{r=ri} \tag{11}$$

$$h=-k\frac{\partial T}{\partial r}\Big)_{r=ri}\frac{1}{(T_w-T_b)} \tag{12}$$

Hence, the Nusselt number becomes:

$$Nu_z = \frac{hD_h}{k} = -\frac{\partial T}{\partial r}\Big)_{r = ri} \frac{D_h}{(T_w - T_b)} \tag{13}$$

Or, in dimensionless form:

$$Nu_z = \frac{2(1-N)}{\Theta_w - \Theta_b} \tag{14}$$

Where;

$$\Theta_b = \frac{\int_N^1 \Theta\, U\, R\, dR}{\int_N^1 U\, R\, dR} \tag{15}$$

The average Nusselt number is defined as:

$$Nu_m = \frac{1}{L}\int_o^L Nu_z\, dz \tag{16}$$

NUMERICAL SOLUTION

A rectangular grid was used for solving the energy equation while a staggered grid was used for solving the coupling of continuity and momentum equations to eliminate the possibility of a checkerboard pressure and velocity pattern. The pressure and temperature are calculated at the solid grid points and the velocities are calculated at the opened and crossed grid points as shown in **Fig.(3)**.

Energy Equation

Using the Alternating Direction Implicit ADI method, the solution of the energy equation may be written as:

The implicit equation in R-direction;

$$a(j)\Theta^*_{(i,j-1)} + b(j)\Theta^*_{(i,j)} + c(j)\Theta^*_{(i,j+1)} = d(j) \tag{17}$$

Where;

$$a(j) = \left(\frac{\Delta\tau}{2\,Pr\,(\Delta R)^2} - \frac{\Delta\tau}{Pr\,R_{(j)}(4\Delta R)} + V_{(i,j)}\frac{\Delta\tau}{(4\Delta R)} \right) \tag{18}$$

$$b(j) = -1 - \left(\frac{\Delta\tau}{Pr\,(\Delta R)^2} \right) \tag{19}$$

$$c(j)=\left(\frac{\Delta\tau}{2\,Pr\,(\Delta R)^2}+\frac{\Delta\tau}{Pr\,R_{(j)}(4\Delta R)}-V_{(i,j)}\frac{\Delta\tau}{(4\Delta R)}\right) \tag{20}$$

$$d(j)=-\Theta^{n}_{(i,j)}-\frac{2\,\Delta\tau\,(1-N)^2}{Pr\,Re^2(\Delta Z)^2}\left(\Theta^{n}_{(i+1,j)}-2\Theta^{n}_{(i,j)}+\Theta^{n}_{(i-1,j)}\right)+\frac{\Delta\tau\,U_{(i,j)}}{(4\Delta Z)}\left(\Theta^{n}_{(i+1,j)}-\Theta^{n}_{(i-1,j)}\right) \tag{21}$$

The implicit equation in Z-direction;

$$a(i)\Theta^{n+1}_{(i-1,j)}+b(i)\Theta^{n+1}_{(i,j)}+c(i)\Theta^{n+1}_{(i+1,j)}=d(i) \tag{22}$$

Where;

$$a(i)=\left(\frac{2\,\Delta\tau\,(1-N)^2}{Pr\,Re^2\,(\Delta Z)^2}+\frac{\Delta\tau\,U_{(i,j)}}{(4\Delta Z)}\right) \tag{23}$$

$$b(i)=-1-\left(\frac{4\,\Delta\tau\,(1-N)^2}{Pr\,Re^2\,(\Delta Z)^2}\right) \tag{24}$$

$$c(i)=\left(\frac{2\,\Delta\tau\,(1-N)^2}{Pr\,Re^2\,(\Delta Z)^2}-\frac{\Delta\tau\,U_{(i,j)}}{(4\Delta Z)}\right) \tag{25}$$

$$\begin{aligned}d(i)=&-\Theta^{*}_{(i,j)}-\frac{\Delta\tau}{2\,Pr\,(\Delta R)^2}\left(\Theta^{*}_{(i,j+1)}-2\Theta^{*}_{(i,j)}+\Theta^{*}_{(i,j-1)}\right)\\&-\frac{\Delta\tau}{Pr\,R_{(j)}\,(4\Delta R)}\left(\Theta^{*}_{(i,j+1)}-\Theta^{*}_{(i,j-1)}\right)+\frac{\Delta\tau\,V_{(i,j)}}{(4\Delta R)}\left(\Theta^{*}_{(i,j+1)}-\Theta^{*}_{(i,j-1)}\right)\end{aligned} \tag{26}$$

Momentum Equation in Z-Direction

Using forward difference in time and central difference in space around point (i+1/2,j) in **Fig.(3)**, **eq.(6)** becomes;

$$U^{n+1}_{(i+\frac{1}{2},j)}=U^{n}_{(i+\frac{1}{2},j)}+A\,\Delta\tau-\frac{\Delta\tau}{\Delta Z}\left(P^{n}_{(i+1,j)}-P^{n}_{(i,j)}\right) \tag{27}$$

Where;

$$\begin{aligned}A=&-\left(\frac{(U\overline{V})^{n}_{(i+\frac{1}{2},j+1)}-(UV)^{n}_{(i+\frac{1}{2},j-1)}}{(2\Delta R)}+\frac{(U^2)^{n}_{(i+\frac{3}{2},j)}-(U^2)^{n}_{(i-\frac{1}{2},j)}}{(2\Delta Z)}\right)+\frac{U^{n}_{(i+\frac{1}{2},j+1)}-2U^{n}_{(i+\frac{1}{2},j)}+U^{n}_{(i+\frac{1}{2},j-1)}}{(\Delta R)^2}\\&+\frac{1}{R_{(j)}}\frac{U^{n}_{(i+\frac{1}{2},j+1)}-U^{n}_{(i+\frac{1}{2},j-1)}}{(2\Delta R)}+\frac{4(1-N)^2}{Re^2}\frac{U^{n}_{(i+\frac{3}{2},j)}-2U^{n}_{(i+\frac{1}{2},j)}+U^{n}_{(i-\frac{1}{2},j)}}{(\Delta Z)^2}+\frac{Gr}{Re}\frac{\Theta^{n}_{(i,j)}}{4(1-N)^2}\end{aligned} \tag{28}$$

At the beginning of each new iteration, $P=P^{*}$. Thus **eq.(27)** becomes;

$$(U^{*})^{n+1}_{(i+\frac{1}{2},j)}=(U^{*})^{n}_{(i+\frac{1}{2},j)}+A^{*}\,\Delta\tau-\frac{\Delta\tau}{\Delta Z}\left(P^{*}_{(i+1,j)}-P^{*}_{(i,j)}\right) \tag{29}$$

Subtracting **eq.(29)** from **eq.(27)**, we have;

$$(U')^{n+1}_{(i+\frac{1}{2},j)} = (U')^{n}_{(i+\frac{1}{2},j)} + A'\Delta\tau - \frac{\Delta\tau}{\Delta Z}\left(P'_{(i+1,j)} - P'_{(i,j)}\right)^{n} \quad (30)$$

Where;

$$(U')^{n+1}_{(i+\frac{1}{2},j)} = U^{n+1}_{(i+\frac{1}{2},j)} - (U^{*})^{n+1}_{(i+\frac{1}{2},j)} \quad (31)$$

$$(U')^{n}_{(i+\frac{1}{2},j)} = U^{n}_{(i+\frac{1}{2},j)} - (U^{*})^{n}_{(i+\frac{1}{2},j)} \quad (32)$$

$$A' = A - A^{*} \quad (33)$$

$$P'_{(i,j)} = P_{(i,j)} - P^{*}_{(i,j)} \quad (34)$$

$$P'_{(i+1,j)} = P_{(i+1,j)} - P^{*}_{(i+1,j)} \quad (35)$$

Following the work of **(Suhas V. Patenkar 1980)**, let us arbitrary set A' and $(U')^{n}$ equal to zero in **eq.(30)**, obtaining;

$$(U')^{n+1}_{(i+\frac{1}{2},j)} = -\frac{\Delta\tau}{\Delta Z}\left(P'_{(i+1,j)} - P'_{(i,j)}\right)^{n} \quad (36)$$

Substituting **eq.(31)** in **eq.(36)** gives;

$$(U)^{n+1}_{(i+\frac{1}{2},j)} = (U^{*})^{n+1}_{(i+\frac{1}{2},j)} - \frac{\Delta\tau}{\Delta Z}\left(P'_{(i+1,j)} - P'_{(i,j)}\right)^{n} \quad (37)$$

Momentum Equation in R-Direction

Using forward difference in time and central difference in space around point (i,j+1/2) in **Fig.(3)**, **eq.(7)** becomes;

$$V^{n+1}_{(i,j+\frac{1}{2})} = V^{n}_{(i,j+\frac{1}{2})} + B\Delta\tau - \frac{Re^{2}}{4(1-N)^{2}}\frac{\Delta\tau}{\Delta R}\left(P^{n}_{(i,j+1)} - P^{n}_{(i,j)}\right) \quad (38)$$

Where;

$$B = -\left(\frac{(V^{2})^{n}_{(i,j+\frac{3}{2})} - (V^{2})^{n}_{(i,j-\frac{1}{2})}}{(2\Delta R)} + \frac{(V\bar{U})^{n}_{(i+1,j+\frac{1}{2})} - (VU)^{n}_{(i-1,j+\frac{1}{2})}}{(2\Delta Z)}\right) + \frac{V^{n}_{(i,j+\frac{3}{2})} - 2V^{n}_{(i,j+\frac{1}{2})} + V^{n}_{(i,j-\frac{1}{2})}}{(\Delta R)^{2}} + \frac{1}{R_{(j+\frac{1}{2})}}\frac{V^{n}_{(i,j+\frac{3}{2})} - V^{n}_{(i,j-\frac{1}{2})}}{(2\Delta R)} - \frac{V^{n}_{(i,j+\frac{1}{2})}}{(R_{(j+\frac{1}{2})})^{2}} + \frac{4(1-N)^{2}}{Re^{2}}\frac{V^{n}_{(i+1,j+\frac{1}{2})} - 2V^{n}_{(i,j+\frac{1}{2})} + V^{n}_{(i-1,j+\frac{1}{2})}}{(\Delta Z)^{2}} \quad (39)$$

At the beginning of each new iteration, P=P*. Thus **eq.(38)** becomes;

$$(V^*)^{n+1}_{(i,j+\frac{1}{2})} = (V^*)^{n}_{(i,j+\frac{1}{2})} + B^*\,\Delta\tau - \frac{Re^2}{4(1-N)^2}\frac{\Delta\tau}{\Delta R}\left(P^*_{(i,j+1)} - P^*_{(i,j)}\right) \tag{40}$$

Subtracting **eq.(40)** from **eq.(38)**, gives;

$$(V')^{n+1}_{(i,j+\frac{1}{2})} = (V')^{n}_{(i,j+\frac{1}{2})} + B'\,\Delta\tau - \frac{Re^2}{4(1-N)^2}\frac{\Delta\tau}{\Delta R}\left(P'_{(i,j+1)} - P'_{(i,j)}\right)^n \tag{41}$$

Where;

$$(V')^{n+1}_{(i,j+\frac{1}{2})} = (V)^{n+1}_{(i,j+\frac{1}{2})} - (V^*)^{n+1}_{(i,j+\frac{1}{2})} \tag{42}$$

$$(V')^{n}_{(i,j+\frac{1}{2})} = (V)^{n}_{(i,j+\frac{1}{2})} - (V^*)^{n}_{(i,j+\frac{1}{2})} \tag{43}$$

$$B' = B - B^* \tag{44}$$

$$P'_{(i,j)} = P_{(i,j)} - P^*_{(i,j)} \tag{45}$$

$$P'_{(i,j+1)} = P_{(i,j+1)} - P^*_{(i,j+1)} \tag{46}$$

Following the work of **(Suhas V. Patenkar 1980)**, let us arbitrary set B' and $(V')^n$ equal to zero in **eq.(41)**, obtaining;

$$(V')^{n+1}_{(i,j+\frac{1}{2})} = -\frac{Re^2}{4(1-N)^2}\frac{\Delta\tau}{\Delta R}\left(P'_{(i,j+1)} - P'_{(i,j)}\right)^n \tag{47}$$

Substituting **eq.(42)** in **eq.(47)** gives;

$$(V)^{n+1}_{(i,j+\frac{1}{2})} = (V^*)^{n+1}_{(i,j+\frac{1}{2})} - \frac{Re^2}{4(1-N)^2}\frac{\Delta\tau}{\Delta R}\left(P'_{(i,j+1)} - P'_{(i,j)}\right)^n \tag{48}$$

Continuity Equation

Writing the continuity equation in the central difference form around (i,j);

$$\frac{V_{(i,j+\frac{1}{2})} - V_{(i,j-\frac{1}{2})}}{\Delta R} + \frac{V_{(i,j)}}{R_{(j)}} + \frac{U_{(i+\frac{1}{2},j)} - U_{(i-\frac{1}{2},j)}}{\Delta Z} = 0 \tag{49}$$

Substituting **eqs.(37) and (48)** in **eq.(49)** and dropping the subscript, we have;

$$P'_{(i,j)} = \frac{-1}{a}\left(bP'_{(i+1,j)} + bP'_{(i-1,j)} + cP'_{(i,j+1)} + cP'_{(i,j-1)} + d\right) \tag{50}$$

Where;

$$a = 2\left(\frac{\Delta\tau\,\Delta R}{\Delta Z} + \frac{Re^2}{4(1-N)^2}\frac{\Delta\tau\,\Delta Z}{\Delta R}\right) \quad (51)$$

$$b = -\frac{\Delta\tau\,\Delta R}{\Delta Z} \quad (52)$$

$$c = -\left(\frac{Re^2}{4(1-N)^2}\frac{\Delta\tau\,\Delta Z}{\Delta R}\right) \quad (53)$$

$$d = \Delta Z\left(V^*_{(i,j+\frac{1}{2})} - V^*_{(i,j-\frac{1}{2})}\right) + \frac{\Delta R\,\Delta Z}{R_{(j)}}V^*_{(i,j)} + \Delta R\left(U^*_{(i+\frac{1}{2},j)} - U^*_{(i-\frac{1}{2},j)}\right) \quad (54)$$

The local Nusselt number **eq.(14)** can be written as;

$$Nu_{(i)} = \frac{2(1-N)}{\Theta_{(i,1)} - \Theta_{b(i)}} \quad (55)$$

Applying Trapezoidal rule to integrate the average Nusselt number **eq.(16)**;

$$Nu_m = \frac{1}{Z}\left(Nu_{(2)} + 2\sum_{i=3}^{i=mt-1} Nu_{(i)} + Nu_{(mt)}\right)\frac{\Delta Z}{2} \quad (56)$$

COMPUTATIONAL ALGORITHM

- Solve **eqs.(17) and (22)** for temperature $\Theta^{n+1}_{(i,j)}$.
- Guess values of $(P^*)^n$ at all the pressure grid points (the filled points in **Fig.(3)**). Also arbitrary set values of $(U^*)^n$ and $(V^*)^n$ at the proper velocity grid points (the open and crossed points in **Fig.(3)**).
- Solve for $(U^*)^{n+1}$ and $(V^*)^{n+1}$ from **eqs.(29) and (40)** respectively at all appropriate interior grid points.
- Using the values of $(U^*)^{n+1}$ and $(V^*)^{n+1}$ obtained in steps 3, solve for (P') from the pressure correction formula, **eq.(50)** by the relaxation technique.
- Calculate $(P)^{n+1}$ at all internal grid points from the following equation;
- $$P^{n+1}_{(i,j)} = (P^*)^n_{(i,j)} + \alpha_p P' \quad (57)$$
    - Where α_p is underrelaxation factor. In the present work, the value of α_p was set as 0.2.
- Calculate (U') and (V') from **eqs.(36) and (47)** respectively.
- The new values of $(U^*)^n$ and $(V^*)^n$ for the next iteration will be obtained by underrelaxate $(U^*)^{n+1}$ and $(V^*)^{n+1}$ obtained in step 3, as follows ;

- $$(U^*)^n = (U^*)^{n+1} + \alpha_p U'$$ (58)
- $$(V^*)^n = (V^*)^{n+1} + \alpha_p V'$$ (59)
- Calculate the average Nusselt Number using **eq.(56)**.
- Repeat steps 1 to 8 until convergence is reached by setting the summation of the mass source term (d) for the entire domain in **eq.(54)** equal to 10^{-4} and by setting the difference in the average Nusselt number Nu_m between the present iteration and the previous iteration equal to 10^{-4}.

EXPERIMENTAL APPARATUS AND PROCEDURES

An experimental rig was designed and constructed by **(Akeel Al−Sudani, 2005)** in the University of Technology and it was used in the present work to study the heat transfer process by mixed convection to a simultaneously hydrodynamic and thermal developing air flow in an inclined annulus. The experimental apparatus is shown in **Fig.(4)**. The present study including the opposing flow position in addition to the aiding flow position with a different inclination angles to those covered by **(Akeel Al−Sudani, 2005)**. The purpose of using this rig was to deduce an empirical equation of average Nusselt number as a function of Reynolds number, Raylieh number, and to compare the theoretical results with the experimental ones.

Experimental Procedure

- The inclination angle of the annulus was adjusted as required.
- The centrifugal fan was then switched on to circulate the air, through the open loop. A regulating valve was used for adjusting the required mass flow rate.
- The electrical heater was switched on and the heater input power then adjusted to give the required heat flux.
- The apparatus was left at least three hours to establish steady state condition. The thermocouples readings were measured every half an hour by means of the digital electronic thermometer until the reading became constant, a final reading was recorded.
- During each test run, the angle of inclination of the annulus in degree, the reading of the manometer (air flow rate) in mm H_2o, the readings of the thermocouples in ˚C, the heater current in amperes and the heater voltage in volts were recorded.

RESULTS AND DISCUSSION

Experimental Results

A total of 51 test runs were carried out to cover annulus inclination angles, horizontal ($\alpha=0^o$), aiding flow ($\alpha=20^o$, 60^o and 90^o) and opposing flow ($\alpha=-20^o$ and -60^o). The heat flux varied from 93 W/m^2 to 857 W/m^2 and Reynolds number varied from 154 to 724.

Heat Flux and Reynolds Number Effect on the Surface Temperature & Nu_z Distribution

Figs.(5) and (6) show the variation of the surface temperature and the local Nusselt number along the inner cylinder for different heat flux and for Re=218. Figures show that the surface temperature and the local Nusselt number increase as

the heat flux increase with constant Reynolds number. This can be attributed to the increasing of the thermal boundary layer faster due to buoyancy effect as the heat flux increases for the same Reynolds number.

Figs.(7) and (8) show the variation of the surface temperature and the local Nusselt number along the inner cylinder for different Reynolds number and for heat flux (258 W/m^2). Figures show that the surface temperature decrease and the local Nusselt number increase as the Re number increase with constant heat flux**.** It is necessary to mention that as heat flux increases the inner tube surface temperature increases because the free convection is the dominating factor in the heat transfer process.

Angle of Inclination Effect on the Surface Temperature & Nu_z Distribution

Figs.(9) and (10) show the influence of inclination angle for aiding flow on the inner cylinder surface temperature and the local Nusselt number distribution for (Re=378, q=379 W/m^2). Figures show a reduction in surface temperature and increasing in the local Nusselt number as the angle of inclination changes from vertical to horizontal position (aiding flow); this can be attributed to the large buoyancy effect in a horizontal annulus compared with the other annulus angle of inclination. The same behavior is found as the angle of inclination changes from negative angles (opposing flow) to horizontal position.

Flow Direction Effect on the Surface Temperature & Nu_z Distribution

Figs.(11) and (12) show the influence of flow direction (i.e., aiding & opposing flow) on the inner cylinder surface temperature and the local Nusselt number distribution for (Re=154, q=258 W/m^2) for ($\alpha=20^o$ and $\alpha=-20^o$). Figures show a reduction in surface temperature and increasing in the local Nusselt number as the angle of inclination changes from negative angles (opposing flow) to the positive angles (aiding flow); this can be attributed to the large buoyancy effect in the positive angles (aiding flow) compared with the negative angles (opposing flow).

Angle of Inclination Effect on Average Nusselt Number

The influence of inclination angle on Nu_m is plotted for both aiding and opposing flow in **Figs.(13) and (14)** for (q=676 W/m^2, Re=308) and (q=517 W/m^2, Re=218); respectively. Figures show that (ζ) decrease as the angle of inclination changes from horizontal position to the positive angles (aiding flow) and from horizontal position to negative angles (opposing flow) due to the decreasing of buoyancy effect as the angle changes from the horizontal position to the inclined position.

Average Nusselt Number versus Reynolds Number and Rayleigah Number

The relationship between average Nusselt number and Reynolds number are plotted in **Figs.(15) and (16)** for ($\alpha=0^o$, q=258 W/m^2), ($\alpha=\pm60^o$, q=676 W/m^2), respectively. Figures show that an increase in the average Nusselt number as Reynolds number increase and the values of the average Nusselt number for aiding flow are greater than that for opposing flow at the same Reynolds number. This can be attributed to the increase of the bouncy effect in the case of aiding flow which improves the heat transfer process.

The relationship between average Nusselt number and Rayleigh number are plotted in **Figs.(17) and (18)** for ($\alpha=0^o$, Re=218), ($\alpha=\pm60^o$, Re=378), respectively. Figures show an increase in the average Nusselt number as Rayleigh number increase and that the values the average Nusselt number for aiding flow are greater than that for opposing flow at the same Rayleigh number. This can be attributed to the increase of the bouncy effect in the case of aiding flow which improves the heat transfer process.

THEORETICAL RESULTS

Temperature Profile

The variation of temperature profiles along the vertical annulus are shown in **Fig.(19)**, for (q=150 W/m^2, Re=1000). Figure shows a steep temperature gradient near the heated surface and the thickness of the thermal boundary layer gradually increases as the flow moves from annulus inlet towards annulus exit.

Velocity Profile

The velocity Profiles show the limitation of the buoyancy effect in the case of Gr/Re=0 see **Fig.(20)**, as all the profiles show approximately similar distribution about the middle of the annular space which is similar to pure forced convection behavior **(Cony and El-Sharrawi 1975)**. **Fig.(21)** shows the development of the axial velocity profiles along the annulus axis for (q=150 W/m^2, Re=1000). It can be seen that the profiles bias slightly towards the heated surface. That can be attributed to the decreasing in the air density near the heated surface which will cause a decrease in the effect of the gravitational body force, which is proportional to the density. **Fig.(22)** shows the effect of the parameter Gr/Re on the axial velocity profile at z=0.603m for Gr/Re=±1898 with Gr/Re=0. It is clear from the this figure that when the free convection opposes the forced flow the buoyancy force tends to retard the fluid near the heated boundary and accelerates it near the opposite adiabatic wall and vice versa, which have the same behavior that found by **(El-Sharrawi and Sarhan 1980)**.

Surface Temperature & Local Nusselt Number

The effect of heat flux and Reynolds number on the surface temperature and the local Nusselt number obtained in the theoretical study is similar to that obtained in the experimental study. **Fig.(23)** shows the effect of the parameter Gr/Re on the local Nusselt number values for Gr/Re=±633 and Gr/Re=±1898 with Gr/Re=0, respectively. It is clear from this figure that with positive values of Gr/Re, the values of local Nusselt number are higher for the same dimensionless axial distance than their corresponding values of the purely forced convection case (Gr/Re=0) and vice versa with the negative values of Gr/Re. This is attributed to the higher velocities near the heated surface, and hence the decrease in the thickness of the developing boundary layer on that boundary, in case of an aiding free convection, which have the same behavior that found by **(El-Sharrawi and Sarhan 1980)**.

Comparison with the Present Theoretical Results

The experimental local Nusselt number results for Re=378, q=258 W/m^2 is compared with the present theoretical results, as shown in **Fig.(24)**. Figure reveals that the experimental local Nusselt number follows the same trend as the present

theoretical results but is approximately higher with maximum difference of 29.47%, minimum difference of 6.46% and mean difference of 17.96%.

CONCLUSIONS

The experimental investigation show that the inner tube surface temperature in the case of aiding flow is lower than that in the case of opposing flow, while the Nu_z value in the case of aiding flow is higher than that in the case of opposing flow (the maximum value occurs in the horizontal position) at the same Reynolds number and heat flux. For the same Reynolds number and annulus orientation, the inner tube surface temperature and the Nu_z increases as the heat flux increases. For the same heat flux and annulus orientation, the inner tube surface temperature increases as the Reynolds number decreases. The theoretical investigation show that The temperature profile along the annulus shows a steep profile near the heated surface with the thermal boundary thickness increases as the heat flux increases, Reynolds number decreases for the same axial position. When the free convection opposes the forced flow the buoyancy force tends to retard the fluid near the heated boundary and accelerates it near the opposite adiabatic wall. But when the free convection aids the forced flow the fluid accelerates near the heated wall and decelerates near the opposite adiabatic boundary, while in the case of Gr/Re=0 (pure forced convection) the maximum velocity occurs at the annular gap centerline (fully developed velocity profile). For constant heat flux the Nu_z value increases at the annulus entrance as Reynolds number increases because of forced convection is dominant, while the Nu_z value increases in the annulus downstream as the Reynolds number decreases due to free convection is dominant. With positive values of Gr/Re the values of Nu_z are higher for the same logarithmic dimensionless axial distance (ZZ) than their corresponding values of the purely forced convection case (Gr/Re=0) and vice versa with the negative values of Gr/Re. The buoyancy effect can be neglected at the annulus entrance for all Reynolds number and heat flux covered in this study.

REFERENCES

- **Akeel A. M. Al−Sudani,** "An investigation into laminar combined convection heat transfer through concentric annuli", PhD. Thesis, University of Technology, Mechanical Engineering Department, September 2005.

- **Cony J. E. R. and El-Shaarawi M. A. I. ,**"Finite difference analysis for laminar flow heat transfer in concentric annuli with simultaneously developing hydrodynamic and thermal boundary layers " , Int. Journal for Numerical Method in Engineering, Vol. 9, pp. 17-38, 1975.

- **El-Shaarawi M. A. and Sarhan A.,** "Free convection effects on the developing laminar flow in vertical concentric annuli ,"J. Heat Transfer, Vol. 102, pp.617-622, November, 1980.

- **John D. Anderson, Jr.,**" Computational Fluid Dynamics"**,** Mc Graw-Hill, New York, 1995**.**

- **Nazrul Islam, Gaitonde U.N. and Sharma G.K.,**" Mixed convection heat transfer in the entrance region of horizontal annuli", Int. J. Heat Mass Transfer. Vol.44, No.11, pp. 2107- 2120, 2001.

- **Suhas V. Patenkar,**"Numerical Heat Transfer and Fluid Flow", Hemisphere, New York, 1980.

NOMENCLATURE

Latin Symbols

SYMBOL	DESCRIPTION	UNITS
D_h	Hydraulic diameter=$2(r_o-r_i)$	m
h	Heat transfer coefficient	$W/m^2.{}^oC$
k	Thermal conductivity	$W/m.{}^oC$
L	Length	m
N	Radius ratio=r_i/r_o	–
p	Pressure	N/m^2
q	Heat flux	W/m^2
r	Radial coordinate	m
r_o	Outer radius of inner cylinder	m
r_i	Inner radius of outer cylinder	m
t	Time	s
T	Temperature	^oC
u	Axial velocity	m/s
v	Radial velocity	m/s
z	Axial coordinate	m

Creak Symbols

α_p	Relaxation factor	–
α	Angle of inclination	degree
$\hat{\alpha}$	Thermal diffusivity	m^2/s
β	Coefficient of volume expansion	1/K
ζ	Average Nusselt number ratio for inclined to horizontal position	–
μ	Dynamic viscosity	kg/m.s
υ	Kinematic viscosity	m^2/s
ρ	Density	kg/m^3

Dimensionless Groups

Gr	Grashof number	$g\beta q r_o D_h^3/\upsilon^2 k$
Nu	Nusselt number	$h D_h/k$
P	Pressure at any cross section	$p-p_i/\rho_i.u_i^2$
Pr	Prandtl number	$\mu.C_p/k$
R	Radial coordinate	r/r_o
Ra	Rayligh number	Gr.Pr
Re	Reynolds number	$u_i.D_h/\upsilon$
Θ	Temperature	$(T-T_i)\ k/q"\ r_o$

τ	Time	$\upsilon t/r_o$
U	Axial velocity component	u/u_i
V	Radial velocity component	$v.r_o/\upsilon$
Z	Axial coordinate	$2z(1-N)/\ r_o Re$
ZZ	Inverse Graetz number	$z/Re.Pr.D_h$

Superscript

*	Intermediate time step
n+1	forward time step
–	average
*	Initial guessed value
'	Difference between two values

Subscript

B	BULK
i	Axial mesh point
j	Radial mesh point
m	Mean
w	Wall
z	Local in axial direction

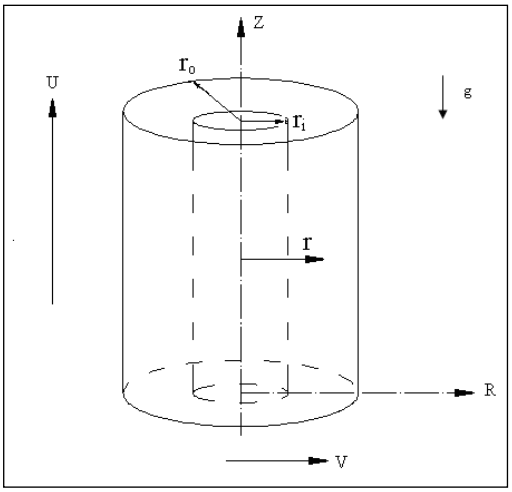

Fig.1: Two-Dimensional Annular Geometry.

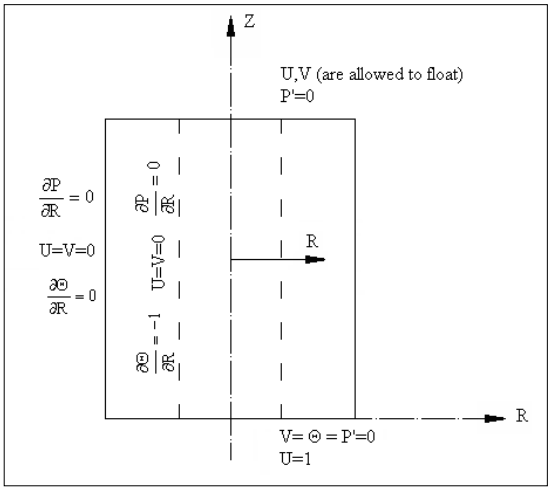

Fig.2: Boundary Conditions

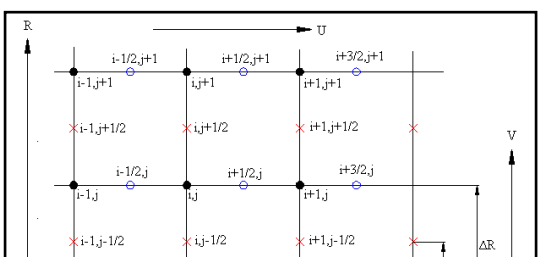

Fig.3: Staggered Mesh Network.

Fig.4: A Photograph of Apparatus.

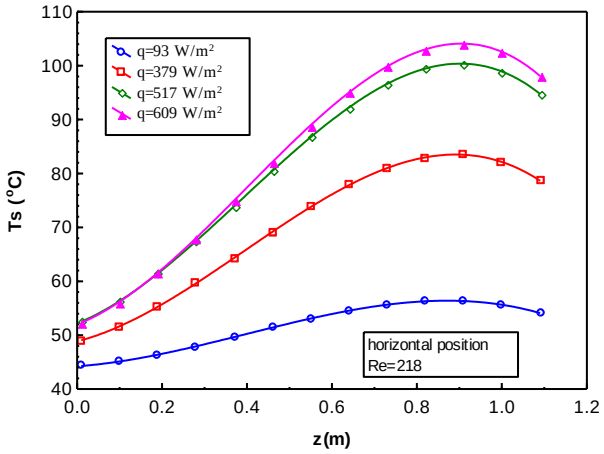

Fig.5: Experimental Variation of the Surface Temperature with the Axial Distance, Re=218, α =0°.

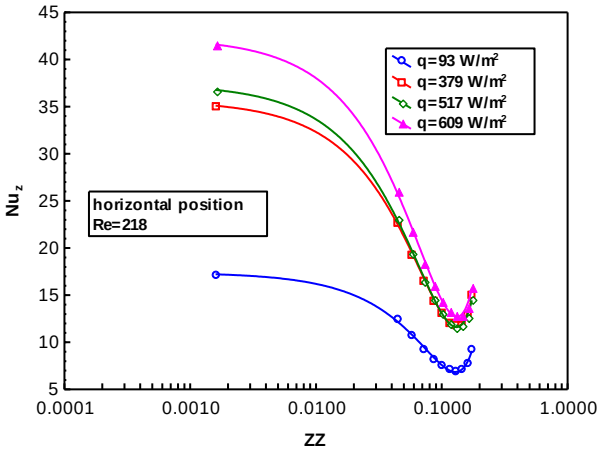

Fig.6: Experimental Local Nusselt Number Versus Dimensionless Axial Distance, Re=218, α =0°.

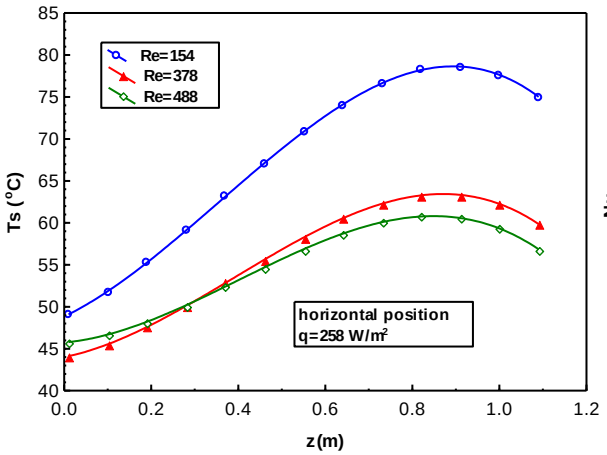

Fig.7: Experimental Variation of the Surface Temperature with the Axial Distance, q=258 W/m², α =0°.

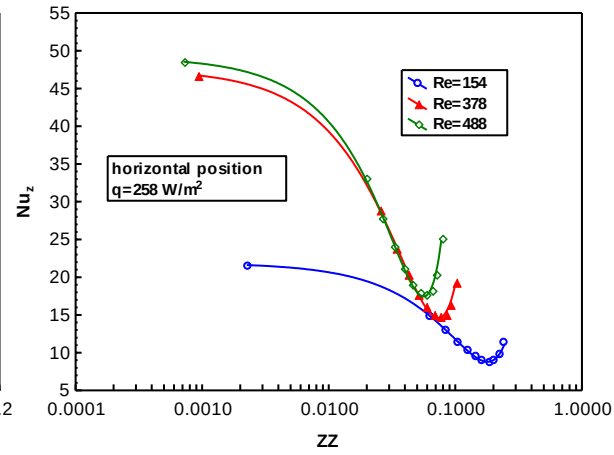

Fig.8: Experimental Local Nusselt Number Versus Dimensionless Axial Distance q=258 W/m², α =0°.

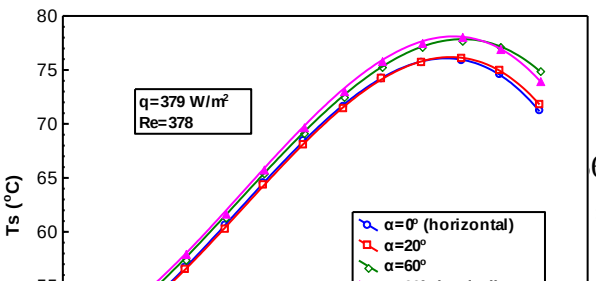

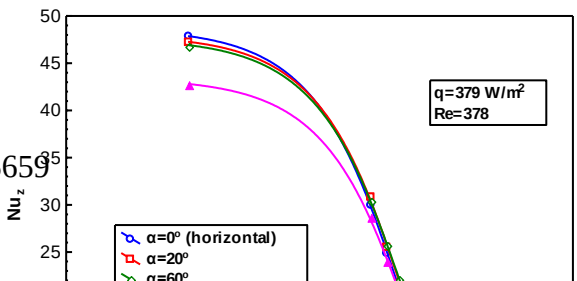

Fig.9: Experimental Variation of the Surface Temperature with the Axial Distance for Various Angles, q=379 W/m^2, Re=378.

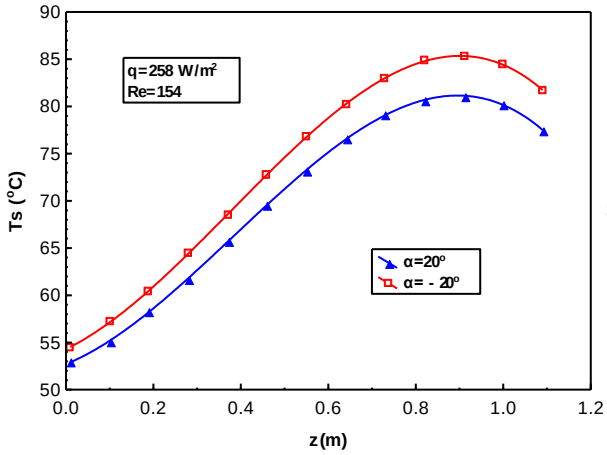

Fig.10: Experimental Local Nusselt Number Versus Dimensionless Axial Distance for Various Angles, q=379 W/m^2, Re=378.

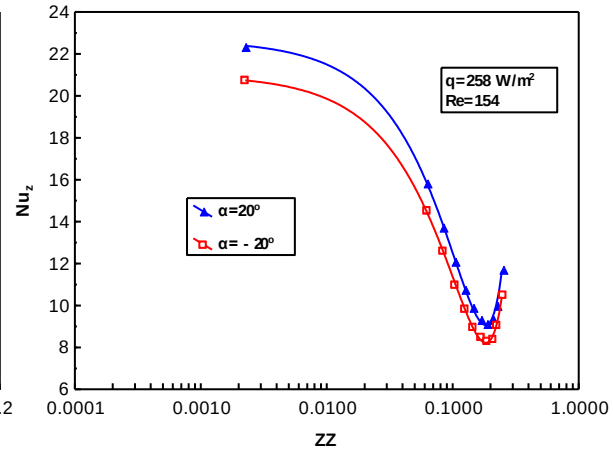

Fig.11: Experimental Variation of the Surface Temperature with the Axial Distance for Various Angles, q=258 W/m^2, Re=154.

Fig.12: Experimental Local Nusselt Number Versus Dimensionless Axial Distance for Various Angles, q=258 W/m^2, Re=154.

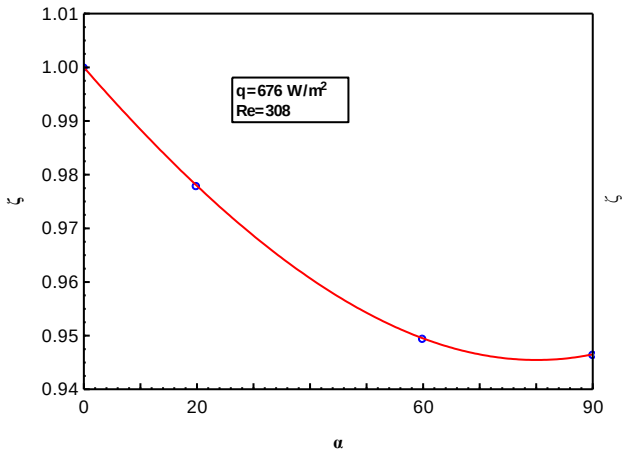

Fig.13: Experimental $\zeta=(Nu_m)_{inc.}/(Nu_m)_{hor}$ as a Function of Inclination Angle for q=676 W/m^2, Re=308 (Aiding Flow).

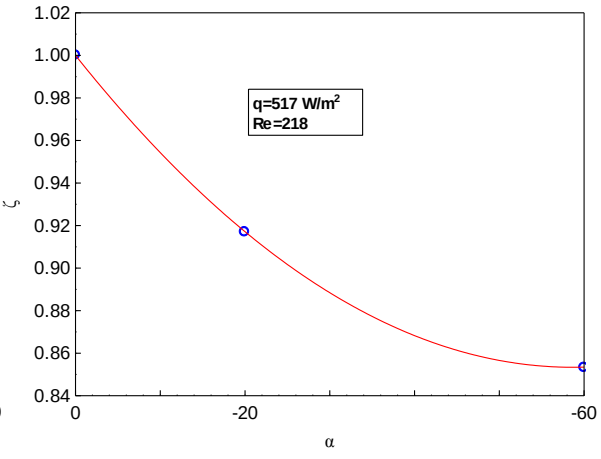

Fig.14: Experimental $\zeta= (Nu_m)_{inc.}/(Nu_m)_{hor}$ as a Function of Inclination Angle for q=517 W/m^2, Re=218 (Opposing Flow).

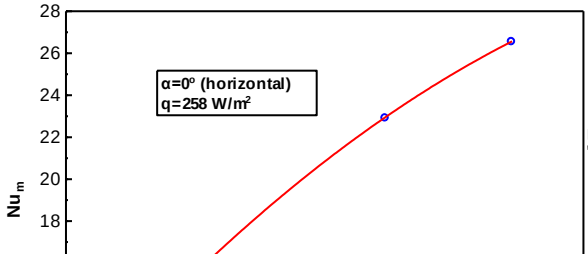

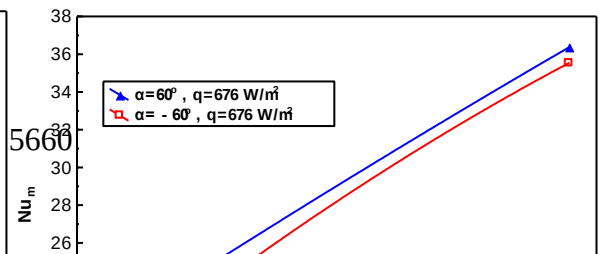

Fig.15: Experimental Average Nusselt Number Versus Reynolds Number for q=258 W/m^2 , α=0^o (Horizontal).

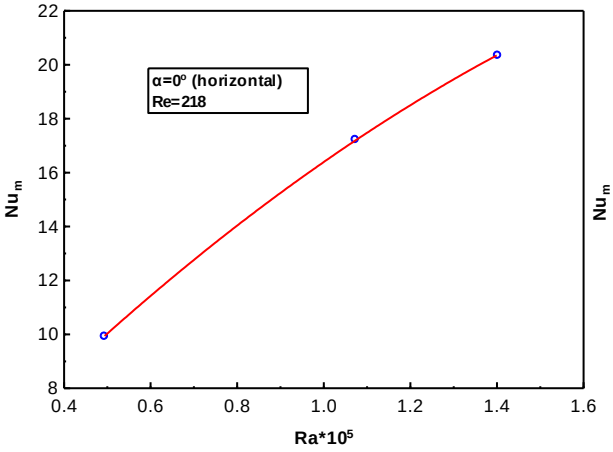

Fig.16: Experimental Average Nusselt Number Versus Reynolds Number for Various Angles, q=676 W/m^2 .

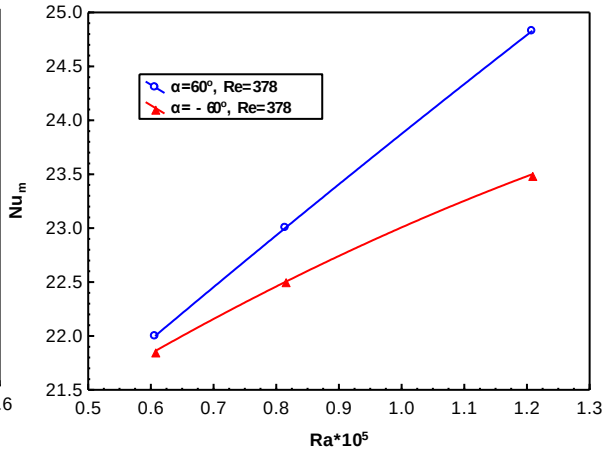

Fig.17: Experimental Average Nusselt Number Versus Rayleigh Number for Re=218, α=0^o (Horizontal).

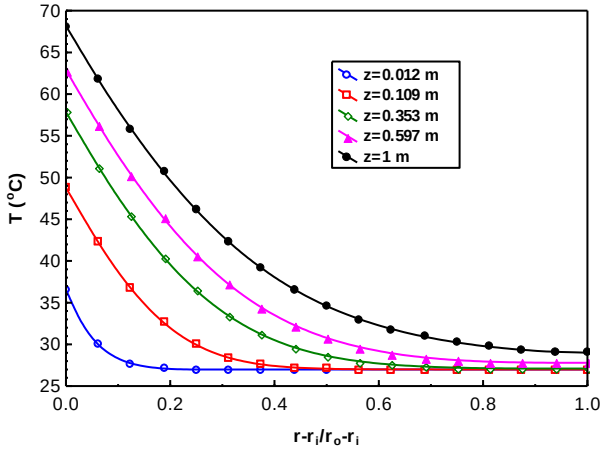

Fig.18: Experimental Average Nusselt Number Versus Rayleigh Number for Various Angles, Re=378.

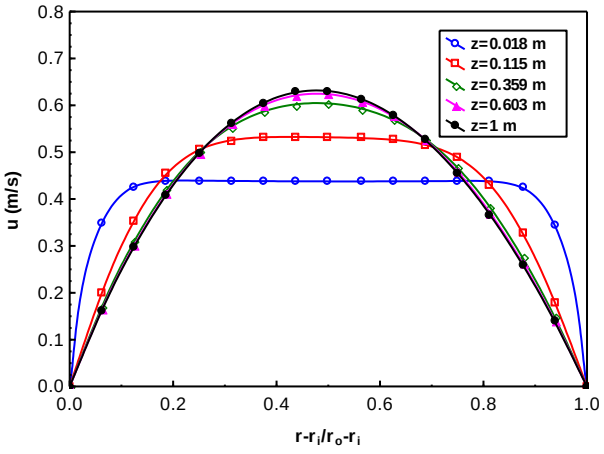

Fig.19: Theoretical Development of the Temperature Profiles Along the Annulus for q=150 W/m^2 , Re=1000.

Fig.20: Theoretical Development of the Axial Velocity Profiles Along the Annulus for Gr/Re=0.

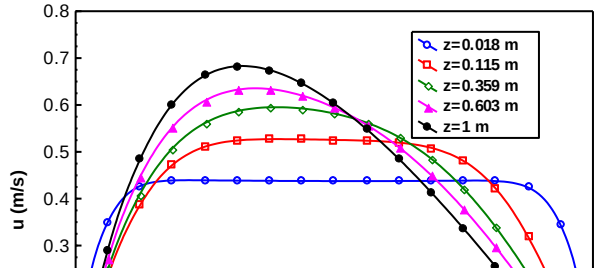

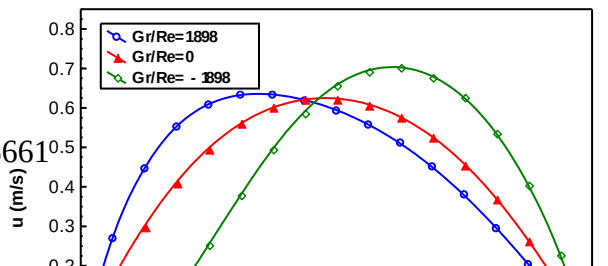

Fig.21: Theoretical Development of the Axial Velocity Profiles Along the Annulus for q=150 W/m^2 , Re=1000.

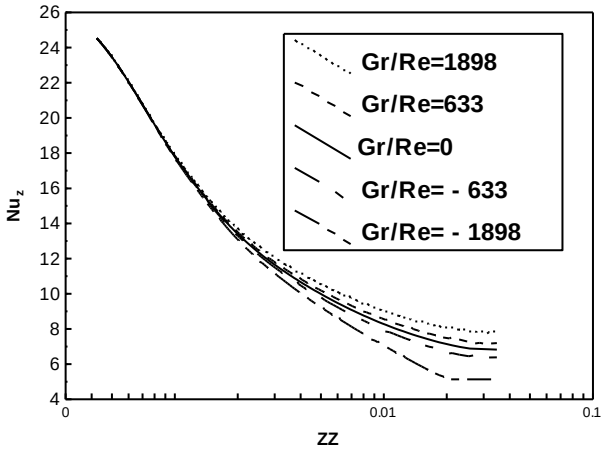

Fig.22: Theoretical Development of the Axial Velocity Profiles at z=0.603m for Various Values of Gr/Re.

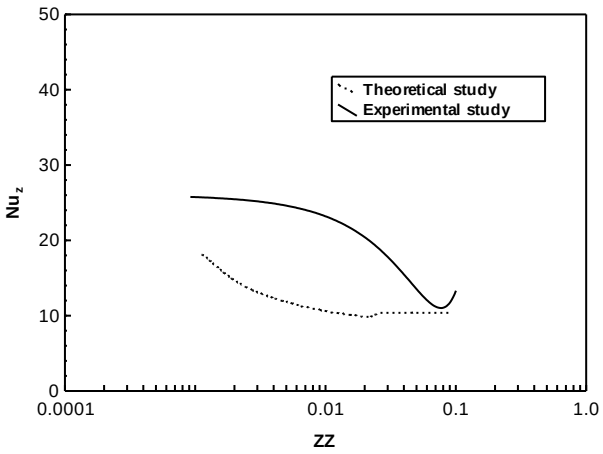

Fig.23: Theoretical Local Nusselt Number Versus Dimensionless Axial Distance for Various Values of Gr/Re.

Fig.24: Comparison of Experimental Nu$_z$ with the Theoretical Result for Vertical Position, q=258 W/m^2 Re=378 .